Journal of Environmental Chemical Engineering 6 (2018) 7021–7028

Contents lists available at ScienceDirect

Journal of Environmental Chemical Engineering

journal homepage: www.elsevier.com/locate/jece

Influence of GO reinforcement on keratin based smart hydrogel and its application for emerging pollutants removal

María Luz Peralta Ramos[a], Gonzalo Galaburri[a], Joaquín Antonio González[a], Claudio Javier Pérez[c], María Emilia Villanueva[a,b], Guillermo Javier Copello[a,b,*]

[a] Universidad de Buenos Aires (UBA), Facultad de Farmacia y Bioquímica, Departamento de Química Analítica y Fisicoquímica, UBA, Junín 956, C1113AAD, Buenos Aires, Argentina
[b] Instituto de Química y Metabolismo del Fármaco, Fac. de Farmacia y Bioquímica, (IQUIMEFA-UBA-CONICET), Argentina
[c] Grupo Ciencia e Ingeniería de Polímeros, Instituto en Investigaciones en Ciencia y Tecnología de Materiales, Universidad de Mar del Plata, CONICET, Juan B. Justo 4302, CP, 7600, Mar del Plata, Argentina

ARTICLE INFO

Keywords:
Smart polymers
Nanocomposites
Keratin
Graphene oxide
Ciprofloxacin remediation

ABSTRACT

In this work, the influence of graphene oxide (GO) reinforcement on keratin based smart hydrogel and its application for the emerging pollutant ciprofloxacin removal was studied. Firstly, the obtained material was characterized by Infrared Spectroscopy, Scanning Electronic Microscopy, Small angle X-ray Scattering and Swelling and Rheological behavior. The results showed that the keratin hydrogel and those nanocomposites containing GO present stimuli responsive behavior by changing the swelling along with the pH. Keratin hydrogels and the ones containing 0.5% of GO showed a similar behavior where swelling decreased between pH 6 and 5. The introduction of GO at 2% changed this inflection point at a value between pH 7 and 6. Also, the swelling of the shrunk hydrogels was higher when containing 2% GO. This effect was probably due to the steric hindrance generated by the nanosheets and their functional groups, partially interfering with keratin chains interaction. The antibiotic was adsorbed in the different active sites in the hydrogel provided by the keratin and the GO structures. After that, the composite adsorption isotherms against ciprofloxacin (CPX) and its kinetics were studied. The ability of the material to expand at high pH allowed a better desorption of the CPX. Thus, reusability presented a better performance when basic washings were used.

1. Introduction

Several contaminants are defined in each country legislation and usually monitored. However, in the past years other contaminants have been found in water bodies. These pollutants are generally produced by pharmaceuticals, daily care and agro-livestock industries, hospital waste, personal hygiene products and therapeutic drugs. These substances, usually hormones, antibiotics and surfactants, are continuously introduced into the environment and are prevalent at small concentrations, which can affect water quality and potentially impact on drinking water supplies, ecosystem and human health.

Ciprofloxacin (CPX) is a fluoroquinolone antibiotic active against gram-positive and gram-negative bacteria and used to treat a wide variety of infections in human and animals. CPX low biodegradability and toxic effects on environmental bacteria have been well documented Moreover, bacteria can develop resistance when antibiotics are in concentrations lower than the minimal inhibitory concentration [1]. CPX had been found in water and wastewater at concentrations typically $< 1\ \mu g\ L^{-1}$ but the concentrations found in the hospital effluents ($3–87\ \mu g\ L^{-1}$) and drug production facilities ($31\ mg\ L^{-1}$) are much higher [1–3] The removal of CPX from wastewater has become an important issue in order to avoid the unwanted consequences in the ecosystems and in the therapeutic uses of this drug.

Many remediation techniques have been described over the past years. Physical remediation methods such as nanofiltration, reverse osmosis, electrodialysis or adsorption with activated carbon, are costly and have maintenance and consumables problems [4–6]. Moreover, few of these techniques can deal with emerging pollutants, such as CPX. Thus, an increment in the use of low cost sorbents, is preferred. Within the low cost and availability biosorbents is keratin [7–10]. It can be obtained from waste materials from the livestock and poultry industry such as hair, wool, hooves, horns, feathers, etc. Due to the characteristics of the material, porous sponge or film-like structures may be obtained which are flexible but with poor mechanical properties for use

* Corresponding author.
E-mail address: gcopello@ffyb.uba.ar (G.J. Copello).

https://doi.org/10.1016/j.jece.2018.11.011
Received 6 July 2018; Received in revised form 8 October 2018; Accepted 4 November 2018
Available online 06 November 2018
2213-3437/

in batch or column systems. Thus, hybrid materials based on keratin have been developed, mainly conjugated with organic counterparts, for example chitosan-keratin, polylactic-keratin, gelatin-keratin [11,12].

The currently reported keratin extraction methodologies have the disadvantage of being costly and only allowing a small portion of the keratin present in the raw material to be recovered. One of the most used techniques described uses a mixture of β-mercaptoethanol, SDS, urea and TRIS and then a dialysis is performed. In this technique a low amount of keratin (20%) is solubilized with a high cost and a negative impact on the environment. However, in a previous work of our group, a pH-responsive keratin hydrogel was obtained by a partial hydrolysis method, using a green friendly technique. The efficiency was around 100%. In this material two extreme states were detected. One at low pH, for which swelling is minimum, and one at high pH, for which swelling is maximum. In addition, the material responsiveness was reversible [13].

The mechanical properties of the keratin gel may also be improved by adding a nanoobject to act as a filler. In this regard, graphene derivatives have gained increased interest. Graphene is a one-atom-thick planar sheet with sp^2 bonded carbon atoms that are densely packed in a honeycomb crystal lattice. Unlike graphene, graphene oxide (GO) has in its structure a large number of functional groups such as hydroxyls, epoxides, carbonyls and carboxyls that increase it solubility in hydrophilic solvents and reactivity. The GO have been extensively used in the past years as a filler and may add adsorption sites to the nanocomposite [14,15]. It is an interesting nanoobject to be included in low-cost adsorbents since it can be obtained from natural graphite. Moreover, other carbon based materials have proven good performance for the removal of CPX by adsorption systems, such as carbon nanotubes, alginate GO hydrogels, together with other nanomaterials such as magnetite nanoparticles [3,16–19] Also, nanomaterials combined with Advanced Oxidation Techniques such as photocatalytic degradation, have been thoroughly studied in the last years [20,21].

The aim of this work was to develop a stimuli-responsive nanocomposite from keratin and GO in order to remediate CPX from wastewater. The obtained material was characterized by Infrared Spectroscopy, Scanning Electronic Microscopy, Small angle X-ray Scattering and Swelling and Rheological behavior. After that, the composite adsorption isotherms, its kinetic behavior against CPX and reusability were studied.

2. Experimental section

2.1. Materials

The bovine horn was kindly provided by Veterinarian Juan Fernandez Pego. Natural graphite powder (< 50 mm particle size) was purchase from Merck (Germany), Water was filtered and deionized with a MilliQ, Millipore system (Milford, MA, USA). The other reagents used were of analytical grade.0

2.2. Graphene oxide (GO) synthesis

Graphite oxide was prepared through Hummers method [22]. Briefly, graphite powder (2.0 *g*) and sodium nitrate (1.0 *g*) were mixed with sulfuric acid (46 mL) in an ice bath with sustained agitation for 4 h. Then, potassium permanganate (6.0 *g*) was added under stirring. The reaction mixture was kept at 35 °C for 2 h. Afterwards, 92 mL of water was added, keeping the solution in the ice bath, and the mixture was further diluted by the addition of 200 mL of water after keeping the temperature at 98 °C for another 2 h. Hydrogen peroxide (20 mL) was then added to reduce the residual potassium permanganate and stirring continued until the mixture turned brown. Finally, the mixture was centrifuged to obtain the graphite oxide powder. In order to clean out any remnants of salt and acid, the powder was re-dispersed in ultrapure water and centrifuged several times. The powder was finally dried at 80 °C. The graphite oxide (30 mg) was exfoliated into GO monolayer nanosheets (nGO) by batch sonication at 35 kHz for 30 min after dispersion in 15 mL of citrate buffer (0.4 M; pH: 4.20). Then, the suspension was centrifuged and the pellet was washed with water and then with methanol. The methanol was removed by heating in an oven at 60 °C and the nGO was then stored at room temperature.

2.3. Preparation of keratin materials

Horn was milled with a file and sieved through a 250 µm sieve. Then, the horn powder was washed three times with distilled water and three times with ethyl acetate to remove fat in mass/volume ratios of 1 *g* powder / 50 mL solvent. After every washing step the powder was centrifuged 5 min at 2000 rpm and the supernatant was discarded. After that, the powder was dried in an oven at 37 °C overnight. Keratin (1 *g*) powder was mixed with 9 ml dilution of NaOH 1 M in Ethanol (25 ml). The mixture was left at 45 °C for 4 h. After that time, it was mixed with different amounts of nGO (in order to obtain a 0.5 and 2.0% w/w nGO hydrogels), the mixtures were homogenized through a syringe and left at 45 °C in an oven until constant mass was achieved. For the preparation of the 0.5 and 2.0% relationships, a nGO stock solution was prepared by weighting 50 mg and suspending in 100 µl of ethanol and sonicating 10 min at 35 kHz. Ten microliters and 20 µl of the nGO ethanolic suspension were added for the KerGO 0.5% and 2% respectively. The final product was a dry block of keratin that was easily hydrated in water to form the hydrogel. The keratin blocks obtained, were thoroughly washed with deonized water in order to remove all NaOH residue. After hydration, the hydrogel form of the material was obtained. Three type of materials were obtained: a keratin hydrogel, named Ker, and two GO containing nanocomposites, named KerGO 0.5% and KerGO 2%.

2.4. Swelling studies

In order to assess the swelling behavior of the material, 0.02 g of a dried material was equilibrated in different 10 mM phosphate solutions ranging from pH 4 to pH 8. After equilibrium was reached, the hydrogels were removed from the solution and accurately weighted.

2.5. Spectroscopic characterization

ATR-FTIR (diamond attenuated total reflectance) of keratin materials were recorded using a Nicolet iS50 Advanced Spectrometer (Thermo Scientific). ATR-FTIR spectra were recorded with 32 scans and a resolution of 4 cm^{-1}.

The investigation of the ultrastructure of the hydrogels swelled at different pH values was performed by Small Angle X-ray Scattering using the SAXS1 beamline of the National Synchrotron Light Laboratory (LNLS), Campinas, Brazil. The SAXS measurements were performed at room temperature in transmission geometry with λ = 1.55 Å (8 keV). The 2D SAXS spectra were monitored using a Pilatus 300 K detector. A sample to-detector distance of 0.9 and 3 m and an exposure time of 60 s were used. The samples were placed with their surfaces perpendicular to the direction of the incident X-ray beam and parallel to the X-ray detector. The scattering intensity (I) was measured as a function of the scattering vector (q) from 0.04 to 2.5 nm^{-1}. The background and parasitic scattering were determined by using an empty sample holder and were subtracted for each measurement.

2.6. Rheological behavior

The rheological behavior of the hydrogels with different GO content were studied. Amplitude sweeps were performed first in order to determine the linear viscoelastic range (LVR). The elastic or storage modulus, G' (ω), the viscous or loss modulus, G'' (ω) and complex viscosity (η^*) of the studied materials were obtained in small-amplitude

oscillatory shear flow experiments using a rotational rheometer from Anton Paar (MCR-301) provided with a CTD 600 thermo chamber. The tests were performed using parallel plates of 25 mm diameter and a frequency range of 0.1–500 s^{-1}. The measurements were carried out at room temperature (20 °C). All the tests were performed using small strains (γ = 0.5%) to ensure the linearity of the dynamic responses. All the runs were repeated using different samples. The gap width used was 700–800 μm.

2.7. Microscopic characterization

Electron microscopy images were obtained on a Zeiss Supra 40 scanning electron microscope (SEM). The hydrogels swelled at different pH were freeze-dried and coated with gold, before the observation.

2.8. CPX adsorption and reuse assays

Ciprofloxacin adsorption behavior was evaluated in batch conditions at 25 °C with constant stirring. The influence of pH, adsorption kinetics and adsorption isotherms were determined. Adsorption capacities, q_{eq} (mg/g) were calculated by sorbate decay in the solution supernatant. In all assays approximately 20 mg of dried material were immersed in 5 mL of CPX containing solutions. Absorbance was measured at 274 nm using an UV–Vis Spectrophotometer (Cecil CE 3021, Cambridge, England). For all experiments the q_{eq} was determined according to the following equation:

$$q_{eq} = (C_0 - C_{eq})V/m \quad (1)$$

where C_0 (mg/L) is the initial concentration, C_{eq} (mg/L) is the equilibrium concentration in the liquid phase, V (L) is the volume of liquid phase, and m (mg) is the mass of the adsorbent. All adsorption assays were carried out in plastic vessels. Blank experiments were conducted in order to verify the absence of sorbate precipitation and/or adsorption to the walls of the vessels. For the evaluation of the pH influence and kinetic behavior a CPX initial concentration of 10 mg/L was used. For the equilibrium assays CPX initial concentrations ranged from 1 to 950 mg/L. Kinetic and equilibrium assays were performed at the optimum adsorption pH (pH 5).

Reuse assays were carried out using the same procedure of the adsorption assays as a first stage. A CPX initial concentration of 10 mg/L at pH 5 was used for the adsorption cycles. After adsorption the materials were transferred to an acid (pH 4) or basic (pH 8) desorption solution and let stand overnight. The samples were dried between cycles in order to accurately determine the swelling. Then, they were transferred to a new CPX containing solution for a second adsorption cycle. This procedure was repeated up to 5 adsorption cycles.

2.9. Point of zero charge determination

The point of zero charge (PZC) of Ker and KerGO nanocomposites was determined by the drift method [23] Briefly, a solution of 0.01 mol L^{-1} NaCl, was boiled to remove dissolved carbon dioxide and used to prepare several solutions with an initial pH ranging from 4 to 8. Then, 0.05 g of the material was added to 10 ml of each solution and incubated at room temperature for 48 h. The final pH was measured and plotted against the initial pH. The pH point at which the curve of the final pH crosses the $pH_{initial} = pH_{final}$ line is the PZC.

2.10. Statistics and graphics

All quantitative results were obtained from triplicate samples. Data were expressed as means ± SD. Statistical analysis was carried out using a two-way ANOVA test and a Bonferroni post-test. A value of $p < 0.05$ was considered to be statistically significant. SAXS 2 D images and scattering profiles were analyzed with Bioxtas Raw. R language and environment was used for statistical computing and graphics [24,25].

3. Results

3.1. Macroscopical characterization

The Ker and KerGO nanocomposites are obtained as dried pieces that can swell to thick hydrogels that withstand handling. Supplementary Data 1 (SD1) shows Ker gel and KerGO 2% nanocomposite in the dry and swelled form. These materials are stiff enough to bear mechanical stirring if they contain up to 2% w/w. GO. KerGO 4% nanocomposites were also tested with unfavorable properties. Although KerGO 4% were macroscopically stiffer than the 2% ones, they were brittle and small grains detached from the edges upon mechanical stirring. The resistance to mechanical stirring, together with the easy manipulation and the high hydration of the gels are remarkable properties when it comes to its applicability in heterogeneous adsorption systems. On one side, the hydrogel form, allows the easy diffusion of solutes within the keratin structure, allowing maximum interaction with the protein functional groups. On the other side, the resistance of the material allows the application on-site and reuse of the systems.

3.2. Rheological behavior

Fig. 1 presents the rheological behavior of Ker and KerGO nanocomposites. All samples showed a gel-like behavior with *G'* values higher than *G''*, meaning that the elastic component is dominant over the viscous component. This dominance of *G'* over *G''* has been widely reported as indicative of the presence of a hydrogel [26]. For practical reasons of requiring a stiff gel for use as a biomaterial, having a material with G' > G'' at all frequencies is usually qualitatively sufficient to characterize how a particular gel will behave in an application [27]. The reinforcement provided by the addition of GO within the keratin structure was evidenced as an increase in *G'* values along with the rise in GO percentage. This would imply that the nanosheets endow the material with greater mechanical strength which will benefit its manipulation of the material when it is introduced and removed for adsorption in heterogeneous phases.

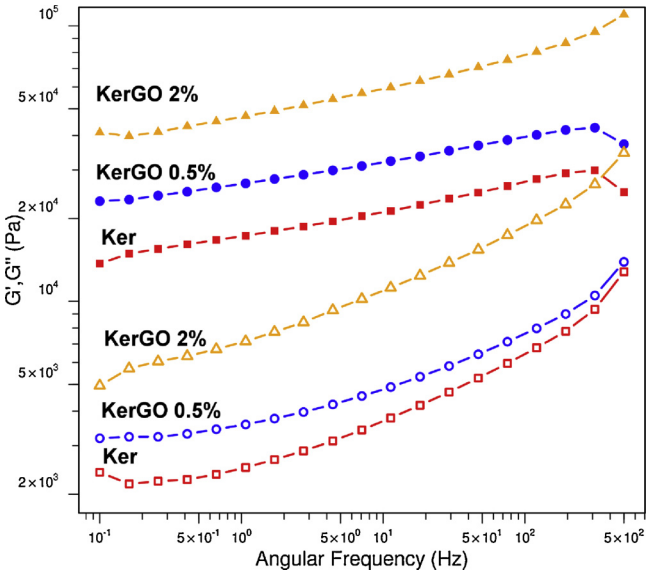

Fig. 1. Frequency dependence of the storage modulus, *G'* (full symbol), and Loss modulus, *G''* (empty symbols), of Ker and KerGO nanocomposites.

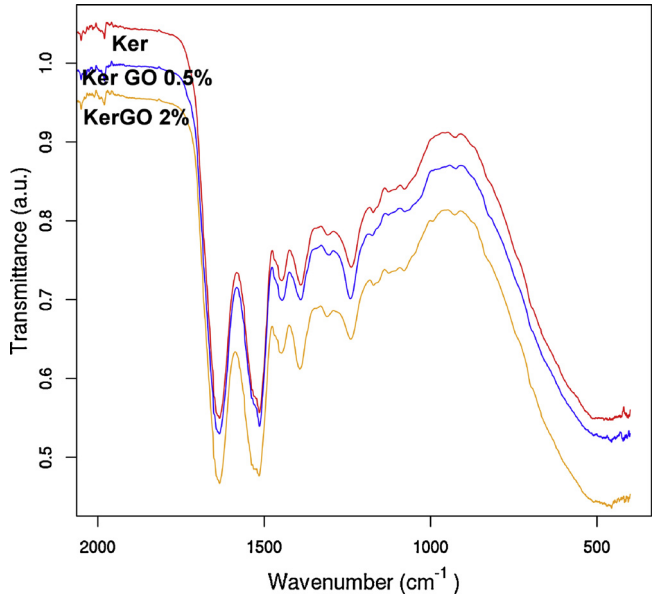

Fig. 2. FT-IR spectra of Ker and KerGO nanocomposites.

3.3. Infrared spectroscopy

Fig. 2, SD2 and SD3 showed the FT-IR spectra of the nGO, Ker, KerGO 0.5% and KerGO 2.0%. In the spectrum of nGO (SD2), the band at 1240 cm^{-1} is attributed to the C—O—C bond stretching which demonstrated the formation of epoxy groups. The presence of carboxyl and carbonyl functional groups could also be detected at 1400 cm^{-1} and 1720 cm^{-1}, which corresponded to C—OH and C═O stretching, respectively [28]. These bands were not present in the KerGOs spectra probably due to the low percentage of the nanoobject. The Ker, KerGO 0.5% and KerGO 2.0% spectra showed no differences between them in regard to new bands. The observed bands correspond to those found in a keratin gel spectrum: amide bands were observed at 1638 cm^{-1}, which corresponded to the elastic vibration of the C═O bond, and at 1535 cm^{-1}, which corresponded to the bending deformation of the C—N—H bond (Fig. 2 and SD3) [29]. When comparing each spectrum, the only appreciable difference is a higher relative intensity of the band at 1392 cm^{-1} respect the 1447 cm^{-1} band, in the KerGO 2.0%. This difference is negligible in Ker and KerGO 0.5% spectra. Being this band related to CH deformation and not present in the GO spectrum, this change in relative intensity can be originated in a keratin structural conformation change introduced by GO at 2% loading.

3.4. Microscopic characterization

Fig. 3 showed the SEM images of the different hydrogels. The topography of the samples was similar in all the cases. Nevertheless, it could be observed that the porous structure partially collapses with the addition of 2% GO. As seen in the FT-IR spectra, the higher GO concentration used introduces detectable variations in the keratin organization whereas the lower concentration used resembles similar to the parent material. In conclusion, the GO presence did not produce a chemical change in the sample but introduced a structural change in the matrix.

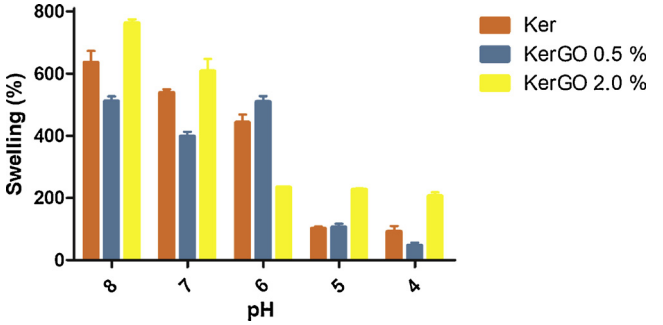

Fig. 4. Swelling behavior at different pH values of Ker and KerGO nanocomposites.

3.5. Swelling behavior and PZC

Fig. 4 showed the swelling behavior of the Ker hydrogel and the KerGO nanocomposites. As it could be seen, all samples present stimuli responsive behavior by changing the swelling % along with the pH. In Ker and KerGO 0.5% samples the behavior was similar: an inflection point was observed between pH 5 and 6, where the swelling % decreased abruptly. However, the introduction of GO at a higher concentration (2%) changed this inflection point at a value between pH 6 and 7.

The pH responsive behavior of the keratin hydrogel mechanism was discussed in a previous work [13]. Briefly, it was proposed that at lower pH values, the keratin structure was collapsed due to the presence of protonated −COOH which were able to establish hydrogen bonds among the protein domains. This interaction allowed the protein chains to closely interact, reducing the material total volume. This lead to a material with low swelling, few pores, and a tight network which interacted with water only by adsorption to its outer hydrophilic sites. On the other hand, at high pH states less interchain hydrogen bonds would be formed in the keratin structure due to deprotonation of carboxyl groups. Thus, higher structure associations would be disfavored and water would be enter within the protein chains in order to hydrate the hydrophylic groups, allowing a higher swelling. This change in swelling is relevant especially between pH 5 and 6 because the pKa of most acid aminoacid is around 4. Regarding the nanocomposites, in the KerGO 0.5% the influence of the GO nanosheets in swelling was negligible. Thus, the swelling behavior was similar to the Ker gel. However, for the KerGO 2% the swelling inflection point shifted to higher pHs probably due to the presence of acidic groups in GO which hinder the aminoacid deprotonation. This was supported by the PZC curves. As can be seen in

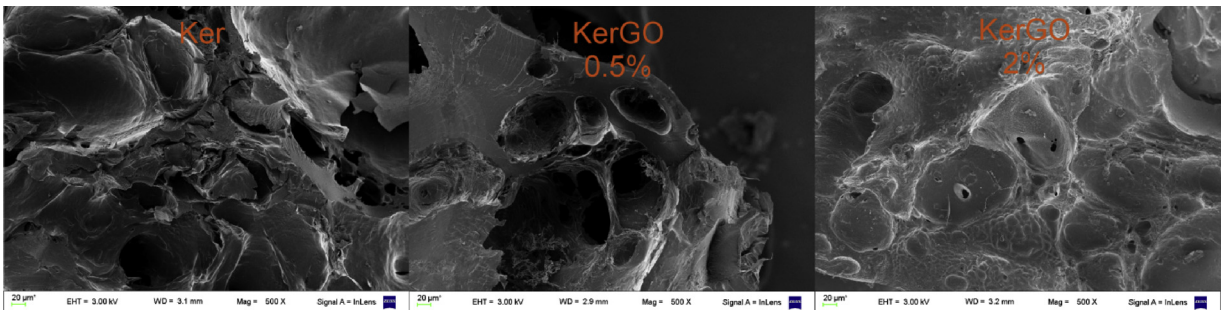

Fig. 3. SEM images of Ker and KerGO nanocomposites.

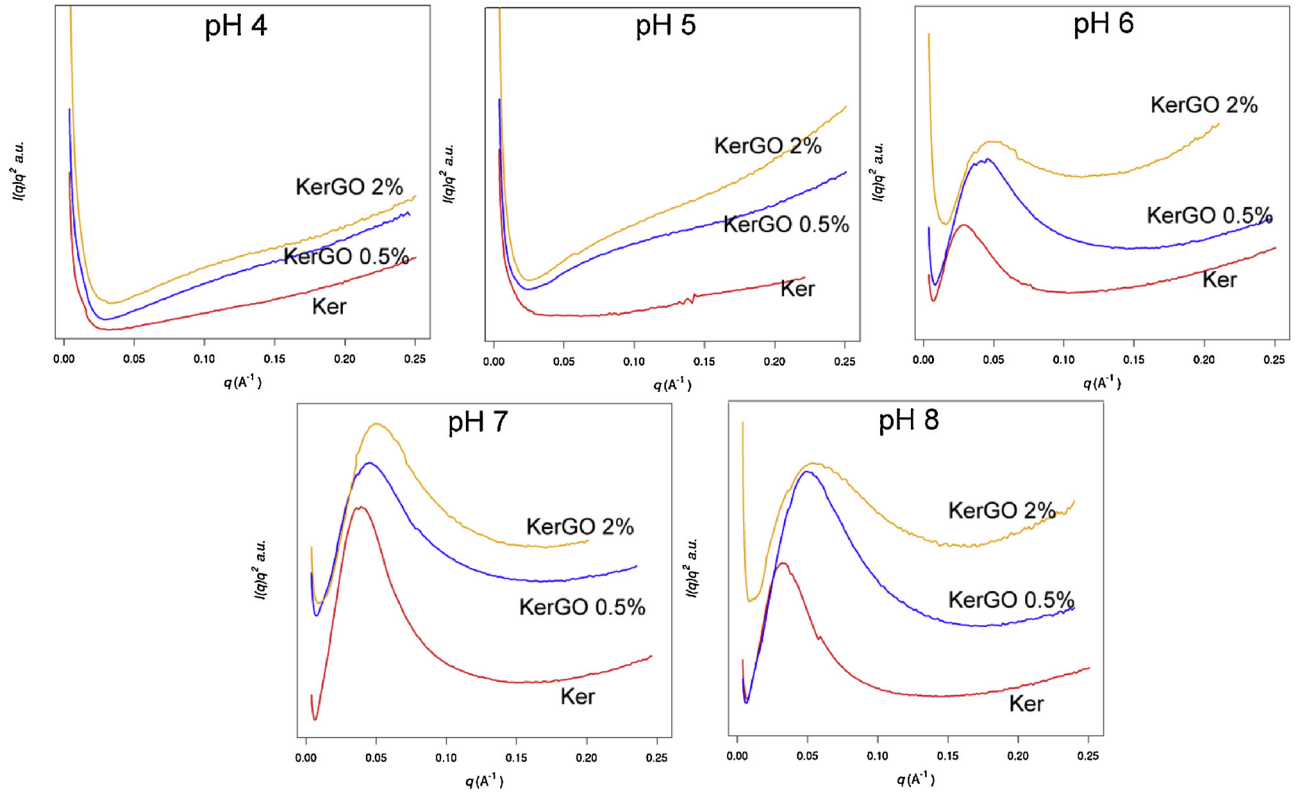

Fig. 5. Kratky representation of SAXS profiles of Ker and KerGO nanocomposites equilibrated at different pHs.

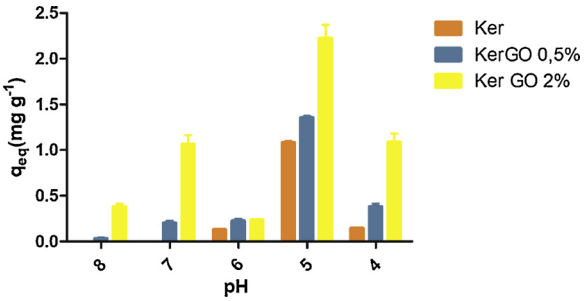

Fig. 6. Effect of media pH in the adsorption of CPX (10 mg/L) on Ker and KerGO nanocomposites.

SD4, With the addition of 0.5% of GO, the PZC of the Ker (7.6) slightly diminishes to a value near pH 7.3. Nevertheless, when 2% of GO is added, the shifts are significant in one pH unit, decreasing to a value around pH 6.6. Thus, in KerGO 2%, the nanocomposites became more negative at lower pHs, due to GO deprotonation rather than aminoacid deprotonation. The presence of more acidic groups nearby the protein acid groups would locally diminish the acidity of the latter leading to the need of higher media pH for the increase in the nanocomposites swelling.

In addition, for KerGO 2% the swelling at the pHs where the structure is collapsed is higher than for the other materials. This, could be due to a higher steric hindrance in keratin chains folding when 2% GO is introduced. This would increase the distance among chain that allowed water to enter between the polypeptide structure.

3.6. Small angle X-ray scattering

Fig. 5 showed the Kratky representation of the SAXS profiles of Ker and KerGO nanocomposites equilibrated at different pHs. The Kratky representation present information from the folding state and flexibility of a protein. As can be seen in Fig. 5, the conformation state of the keratin in the nanocomposites at the different pHs is different from the pristine keratin. This is probably generated by the impossibility of the chains to fully interact when the nanosheets are present. At higher pHs, a peak around 0.05 nm^{-1} indicates the presence of a local organization of similar spatial dimensions in all materials. Nevertheless, for the nanocomposite this structure shifts to higher q which means smaller structures. Also, this peak is broader for the nanocomposites. This indicates that the introduction of GO is interfering with keratin organization, at the both levels tested.

3.7. Ciprofloxacin adsorption at different pH values

The performance of the nanocomposites as adsorbents was evaluated using CPX. The effect of CPX adsorption at pH values of 4.0 to 8.0 was evaluated (Fig. 6). The adsorption capacity was significantly higher at pH 5 than for higher and lower pHs. Above the pKa (6.09) of the CPX carboxylic groups, the repulsion between them and the keratin and GO deprotonated acidic groups became relevant. This effect is expressed as very low adsorption capacities for Ker and KerGO 0.5% nanocomposites [30]. Below pH 4 both the protein and the CPX carboxilic groups would be protonated, diminishing the interaction. Also, at lower pHs a certain repulsion was also expected due to the protonation of the basic groups in the aminoacids and the CPX amino (pKa 8.74 for the nitrogen on the piperazinyl ring) [30]. Thus, CPX is adsorbed at a pH where the equilibrium of charged groups from keratin and GO results in the electrostatic attraction between their carboxilates and protonated amino groups from CPX with minimum repulsion due to a low proportion of carboxilates from the antibiotic. Thus, the presence of negatively charged groups in GO could be the reason of the increment of the adsorption capacities of the nanocomposites respect the Ker gel. Also, the difference in the adsorption capacity observed between KerGO 0.5% and 2% could be originated in the steric hindrance introduced by GO between keratin chains which could lead to more accessible interaction sites and, therefore, higher capacities. Solutions equilibrated at pH 5

Table 1
Kinetic model parameters.

Model	Parameter	Ker	KerGO 0.5%	KerGO 2%
Pseudo-1st order	q_e (μg/g)	(529 ± 14)	689 ± 26	$(1.19 \pm 0.02)\times10^{3}$
	k_1 (h^{-1})	1.3 ± 0.1	0.7 ± 0.1	0.65 ± 0.04
	AICc	434.77	497.65	606.53
Pseudo-2nd order	q_e (μg/g)	$(6.3 \pm 0.3)\times10^{2}$	$(8.2 \pm 0.5)\times10^{2}$	$(1.52 \pm 0.06)\times10^{3}$
	k_2 (g/(μg.h))	$(2.5 \pm 0.5)\times10^{-3}$	$(1.0 \pm 0.3)\times10^{-3}$	$(4.1 \pm 0.6)\times10^{-4}$
	AICc	449.03	497.45	621.87
Elovich	α (μg/(g.h))	$(1.7 \pm 0.6)\times10^{3}$	$(1.2 \pm 0.4)\times10^{3}$	$(1.3 \pm 0.2)\times10^{3}$
	β (g/μg)	$(7 \pm 1)\times10^{-3}$	$(5.3 \pm 0.7)\times10^{-3}$	$(2.4 \pm 0.2)\times10^{-3}$
	AICc	461.788	499.93	637.74
Modified Freundlich	k_f (L/(μg. h))	350 ± 16	369 ± 25	566 ± 25
	m	3.3 ± 0.5	3.0 ± 0.4	2.4 ± 0.2
	AICc	470.87	505.04	659.03

were used for kinetic and isotherm assays.

3.8. Adsorption kinetics

The materials' adsorption capacities over time, presented in SD5, were analyzed by comparing the kinetic behavior adjustment to the pseudo-first order, pseudo-second order, Elovich and modified Freundlich models in their non-linear forms. Table 1 summarizes each material parameters for every model. The mathematical kinetic models and their summary are presented in Supplementary Data. The goodness-of-fit was determined by the corrected Akaike's information criteria (AICc). Smaller AICc values represent better curve fittings. For all samples, adsorption equilibrium was achieved within four hours. According to the pseudo-first and pseudo-second order adsorption rate parameters Ker hydrogels presented a higher adsorptive rate than the KerGO. Nevertheless, the equilibrium concentration for Ker hydrogels was lower. This could be due to a lower mobility of keratin chains in KerGO respect to Ker because of their interaction with GO and probably because of steric hindrance when it comes to the expansion of the network that make available the adsorption sites.

The adsorption rate on GO is lower than in keratin while adsorption capacity is greater. For all samples, the model that fitted better was the pseudo-first order which could indicate that the adsorption rate would be dominated by one main step. Since the *m* parameter of the Modified Freundlich's model was in all cases far from a value of 2, this dominant step would not be related to intraparticle diffusion [31]. Thus, probably the adsorption step would be leading the kinetic rate.

3.9. Adsorption isotherms

Ciprofloxacin adsorption isotherms were obtained after equilibrium time at pH 5. Data was fitted using to two and three parameters isotherm models: Two parameters: Langmuir, Freundlich and Dubinin–Radushkevich (D−R) models; three parameters: Redlich–Peterson (R−P) and Sips models. Adsorption equilibrium data is presented in SD6 and Table 2 presents the results obtained from the fitted models. The mathematical models are presented in Supplementary Data. Since KerGO 2% contains a greater amount of GO, it was expected that this material will present the greater adsorption capacity. Nevertheless, both Langmuir and Sips maximum capacity parameters showed to be greater for the KerGO 0.5%. This could be due to the presence of GO nanosheets stacking in KerGO 2%. Stacking will produce the unavailability of the internal binding sites of the nanosheets. Thus, at low sorbate concentrations KerGO 2% presents higher capacities than KerGO 0.5%, which could be due to a higher number of peripheral binding sites. On the contrary, when higher amounts of sorbates are used as initial concentration, peripheral groups became saturated and the occupation of internal binding sites in KerGO 2% would be unreachable, whereas due to a higher dispersibility, internal groups of GO sheets in KerGO 0.5% would be available leading to higher adsorption capacities. For other GO containing nanocomposites, as Zn-GO-nanocellulose maximum capacities of 10.86 mg/g were reported [32]. On the other hand, studies involving GO and carboxylic polymers, such as sodium and calcium alginate, reported higher *qmax*, 66.25 and 86.12 mg/g respectively, probably due to the contribution of carboxylates from GO and the alginate [17,19]. Literature also present reports with higher CPX maximum adsorption capacities, typically for materials with high GO content such as chitin-GO nanocomposites containing 25%w/w GO [14].

The mean free energy of adsorption can be indicative of the type of adsorption interaction. Its value can be estimated from the parameter of Dubinin-Radushkevich parameter E_{DR}. When chemisorption is the main mechanism of adsorption, E_{DR} value is in the range of 8–16 kJ/mol, as the case for the KerGO nanocomposites, and lower values would indicate physisorption. This means that CPX would be mainly interacting by a charge associated mechanism rather than a physisorption interaction such as π-π stacking with the unsaturated hexagonal rings of nGO.

3.10. Reuse assays

The reutilization of the material was studied by intercalating adsorption and desorption cycles. Two different desorption solutions were assayed: an acid solution at pH 4 and 8. Fig. 7 shows the q_{eq} in different adsorption cycles. It can be observed that the capacity presents lower decays among cycles in those gels desorbed at pH 8. This could have been due to the stimuli-responsive behavior of the material. At high pH, the greater expansion of the gel net, would lead to a desorption equilibrium. The KerGO 2% treated at pH 8 showed the better performance, since it had the higher capacity through the different cycles.

4. Conclusions

The reinforcement of a keratin based smart material was achieved by the introduction of GO nanosheets. The addition of GO would not alter the interaction between the keratin chains, thus maintaining the 3D integrity of the material. Moreover, even after being dry, the material can swell in contact with water. Due to the lack of detection of strong interactions or new covalent bonds, it was proposed that the GO is acting as a filler. Also an important feature of the nanocomposite, the pH-responsive behavior was maintained regardless the introduction of the nanoobject. Nevertheless, inflection point of swelling for the KerGO 2% nanocomposites shifted to higher pHs probably due to the influence of GO acidic groups.

The changes in the keratin structure by the addition of GO were evidenced by the SAXS experiments, showing that the introduction of GO is interfering with keratin organization. The nanocomposites also showed a greater mechanical strength which will benefit the manipulation of the material when it is introduced and removed for adsorption in heterogeneous phases.

Table 2
Isotherm model parameters.

Model	Parameter	KerGO 0.5%	KerGO 2%
Langmuir	q_m (mg/g)	55 ± 6	28 ± 3
	k_a (L/mg)	(6 ± 2)×10^{-3}	(4 ± 1)×10^{-3}
	AICc	152.78	204.29
Sips	q_{mS} (mg/g)	43 ± 1	31 ± 8
	K_S (L/mg)	(9.3 ± 0.5)×10^{-3}	(4 ± 2)×10^{-3}
	n_S	3.3 ± 0.6	0.9 ± 0.2
	AICc	127.55	206.38
Redlich-Peterson	K_{RP} (L/mg)	0.3 ± 0.2	0.14 ± 0.05
	α_{RP} ((L/mg)^{nRP})	0.006 ± 0.02	0.005 ± 0.01
	n_{RP}	1 ± 0.3	1.0 ± 0.3
	AICc	155.45	206.64
Dubinin-Radushkevich	q_{DR} (mg/g)	201 ± 58	95 ± 17
	K_{DR} (mol^2/kJ^2)	(4.51 ± 0.74)×10^{-3}	(4.5 ± 0.5)×10^{-3}
	E_{DR} (kJ/mol)	10.5 ± 0.9	10.5 ± 0.5
	AICc	162.84	207.03
Freundlich	k (L/g h)	2 ± 1	0.9 ± 0.3
	n	0.48 ± 0.08	0.48 ± 0.05
	AICc	166.44	210.47

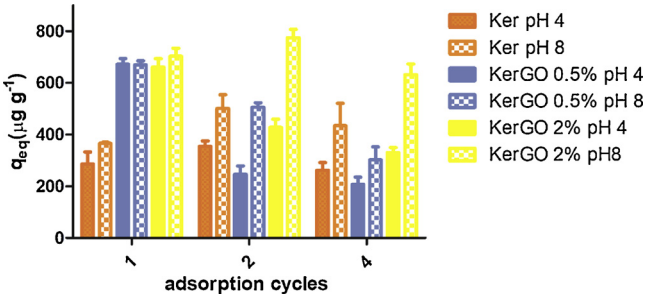

Fig. 7. Reusability of Ker and KerGO nanocomposites using acid or basic washing cycles.

The emergent contaminant, CPX, adsorption to the nanocomposite was studied. Probably the mechanism of adsorption is related to electrostatic attraction.

The reuse of this material was also studied. The treatment with bases achieved the best performance benefited from the pH-responsiveness of the material. This might be due to the expansion that the keratin gel net suffers at high pH values, leading to a higher interaction between the CPX and the solvent.

Acknowledgments

G.G. is grateful for his undergraduate fellowship granted by Universidad de Buenos Aires (UBA). J.A.G. is grateful for his doctoral fellowship granted by Consejo Nacional de Investigaciones Científicas y Técnicas (CONICET). M.E.V. is grateful for her postdoctoral fellowship granted by CONICET. The authors are grateful to the Brazilian Synchrotron Light Laboratory (LNLS) for SAXS facilities and would like to acknowledge INTI Mecánica and M. Pianetti for their assistance in SEM analysis. This work was supported with grants from Universidad de Buenos Aires (UBACYT 20020130100780BA) and Agencia Nacional de Promoción Científica y Tecnológica (PICT 2015-0714, PICT 2016-1997).

Appendix A. Supplementary data

Supplementary material related to this article can be found, in the online version, at doi:https://doi.org/10.1016/j.jece.2018.11.011.

References

[1] D.G.J. Larsson, C. de Pedro, N. Paxeus, Effluent from drug manufactures contains extremely high levels of pharmaceuticals, J. Hazard. Mater. 148 (2007) 751–755, https://doi.org/10.1016/j.jhazmat.2007.07.008.
[2] J. Fick, H. Söderström, R.H. Lindberg, C. Phan, M. Tysklind, D.G.J. Larsson, Contamination of surface, ground and drinking water from pharmaceutical production, Environ. Toxicol. Chem. 28 (2009) 2522, https://doi.org/10.1897/09-073.1.
[3] S.A.C. Carabineiro, T. Thavorn-Amornsri, M.F.R. Pereira, J.L. Figueiredo, Adsorption of ciprofloxacin on surface-modified carbon materials, Water Res. 45 (2011) 4583–4591, https://doi.org/10.1016/j.watres.2011.06.008.
[4] G.M. Gadd, Biosorption: critical review of scientific rationale, environmental importance and significance for pollution treatment, J. Chem. Technol. Biotechnol. 84 (2009) 13–28.
[5] J.S. George, A. Ramos, H.J. Shipley, Tanning facility wastewater treatment: analysis of physical–chemical and reverse osmosis methods, J. Environ. Chem. Eng. 3 (2015) 969–976, https://doi.org/10.1016/j.jece.2015.03.011.
[6] M. Kamrani, A. Akbari, A. Yunessnia lehi, Chitosan-modified acrylic nanofiltration membrane for efficient removal of pharmaceutical compounds, J. Environ. Chem. Eng. 6 (2018) 583–587, https://doi.org/10.1016/j.jece.2017.12.044.
[7] P. Gao, Z. Liu, X. Wu, Z. Cao, Y. Zhuang, W. Sun, G. Xue, M. Zhou, Biosorption of Chromium(VI) Ions by Deposits Produced from Chicken Feathers after Soluble Keratin Extraction, CLEAN – Soil Air Water 42 (2014) 1558–1566, https://doi.org/10.1002/clen.201300669.
[8] P. Gao, K. Li, Z. Liu, B. Liu, C. Ma, G. Xue, M. Zhou, Feather keratin deposits as biosorbent for the removal of methylene blue from aqueous solution: equilibrium, kinetics, and thermodynamics studies, Water Air Soil Pollut. 225 (2014) 1–13, https://doi.org/10.1007/s11270-014-1946-5.
[9] F. Banat, S. Al-Asheh, D. Al-Rousan, Comparison between different keratin-composed biosorbents for the removal of heavy metal ions from aqueous solutions, Adsorpt. Sci. Technol. 20 (2002) 393–416, https://doi.org/10.1260/02636170260295579.
[10] M.A. Khosa, J. Wu, A. Ullah, Chemical modification, characterization, and application of chicken feathers as novel biosorbents, RSC Adv. 3 (2013) 20800–20810, https://doi.org/10.1039/C3RA43787F.
[11] T. Tanabe, N. Okitsu, A. Tachibana, K. Yamauchi, Preparation and characterization of keratin–chitosan composite film, Biomaterials 23 (2002) 817–825, https://doi.org/10.1016/S0142-9612(01)00187-9.
[12] H. Zhang, J. Liu, Electrospun poly(lactic-co-glycolic acid)/wool keratin fibrous composite scaffolds potential for bone tissue engineering applications, J. Bioact. Compat. Polym. 28 (2013) 141–153.
[13] M.L. Peralta Ramos, J.A. González, L. Fabian, C.J. Pérez, M.E. Villanueva, G.J. Copello, Sustainable and smart keratin hydrogel with pH-sensitive swelling and enhanced mechanical properties, Mater. Sci. Eng. C 78 (2017) 619–626, https://doi.org/10.1016/j.msec.2017.04.120.
[14] J.A. González, M.E. Villanueva, L.L. Piehl, G.J. Copello, Development of a chitin/graphene oxide hybrid composite for the removal of pollutant dyes: adsorption and desorption study, Chem. Eng. J. 280 (2015) 41–48, https://doi.org/10.1016/j.cej.2015.05.112.
[15] H. Basu, R.K. Singhal, M.V. Pimple, S. Saha, Graphene oxide encapsulated in alginate beads for enhanced sorption of uranium from different aquatic environments, J. Environ. Chem. Eng. 6 (2018) 1625–1633, https://doi.org/10.1016/j.jece.2018.01.065.
[16] S. Rakshit, D. Sarkar, E.J. Elzinga, P. Punamiya, R. Datta, Mechanisms of ciprofloxacin removal by nano-sized magnetite, J. Hazard. Mater. 246–247 (2013) 221–226, https://doi.org/10.1016/j.jhazmat.2012.12.032.
[17] S. Wu, X. Zhao, Y. Li, C. Zhao, Q. Du, J. Sun, Y. Wang, X. Peng, Y. Xia, Z. Wang, L. Xia, Adsorption of ciprofloxacin onto biocomposite fibers of graphene oxide/calcium alginate, Chem. Eng. J. 230 (2013) 389–395, https://doi.org/10.1016/j.cej.2013.06.072.
[18] H. Li, D. Zhang, X. Han, B. Xing, Adsorption of antibiotic ciprofloxacin on carbon

nanotubes: pH dependence and thermodynamics, Chemosphere 95 (2014) 150–155, https://doi.org/10.1016/j.chemosphere.2013.08.053.
[19] Y. Fei, Y. Li, S. Han, J. Ma, Adsorptive removal of ciprofloxacin by sodium alginate/graphene oxide composite beads from aqueous solution, J. Colloid Interface Sci. 484 (2016) 196–204, https://doi.org/10.1016/j.jcis.2016.08.068.
[20] J. Zhao, Z. Zhao, N. Li, J. Nan, R. Yu, J. Du, Visible-light-driven photocatalytic degradation of ciprofloxacin by a ternary Mn2O3/Mn3O4/MnO2 valence state heterojunction, Chem. Eng. J. 353 (2018) 805–813, https://doi.org/10.1016/j.cej.2018.07.163.
[21] M.E. Villanueva, G.J. Copello, V. Campo Dall'Orto, Solar light efficient photocatalytic activity degradation of emergent contaminants by coated TiO_2 nanoparticles, New J. Chem. (2018), https://doi.org/10.1039/C8NJ02332H.
[22] W.S. Hummers, R.E. Offeman, Preparation of graphitic oxide, J. Am. Chem. Soc. 80 (1958) 1339, https://doi.org/10.1021/ja01539a017.
[23] M.V. Lopez-Ramon, F. Stoeckli, C. Moreno-Castilla, F. Carrasco-Marin, On the characterization of acidic and basic surface sites on carbons by various techniques, Carbon 37 (1999) 1215–1221, https://doi.org/10.1016/S0008-6223(98)00317-0.
[24] S.S. Nielsen, K.N. Toft, D. Snakenborg, M.G. Jeppesen, J.K. Jacobsen, B. Vestergaard, J.P. Kutter, L. Arleth, R.A.W. BioXTAS, A software program for high-throughput automated small-angle X-ray scattering data reduction and preliminary analysis, J. Appl. Crystallogr. 42 (2009) 959–964, https://doi.org/10.1107/S0021889809023863.
[25] R Development Core Team, R: A Language and Environment for Statistical Computing, R Foundation for Statistical Computing, Vienna, Austria, 2009http://www.R-project.org.
[26] K. González, C. García-Astrain, A. Santamaria-Echart, L. Ugarte, L. Avérous, A. Eceiza, N. Gabilondo, Starch/graphene hydrogels via click chemistry with relevant electrical and antibacterial properties, Carbohydr. Polym. 202 (2018) 372–381, https://doi.org/10.1016/j.carbpol.2018.09.007.
[27] C. Yan, D.J. Pochan, Rheological properties of peptide-based hydrogels for biomedical and other applications, Chem. Soc. Rev. 39 (2010) 3528, https://doi.org/10.1039/b919449p.
[28] R. Li, C. Liu, J. Ma, Studies on the properties of graphene oxide-reinforced starch biocomposites, Carbohydr. Polym. 84 (2011) 631–637, https://doi.org/10.1016/j.carbpol.2010.12.041.
[29] P. Kakkar, B. Madhan, G. Shanmugam, Extraction and characterization of keratin from bovine hoof: a potential material for biomedical applications, Springer Plus 3 (2014) 596, https://doi.org/10.1186/2193-1801-3-596.
[30] K. Torniainen, S. Tammilehto, V. Ulvi, The effect of pH, buffer type and drug concentration on the photodegradation of ciprofloxacin, Int. J. Pharm. 132 (1996) 53–61, https://doi.org/10.1016/0378-5173(95)04332-2.
[31] T.S. Anirudhan, S.R. Rejeena, A.R. Tharun, Preparation, characterization and adsorption behavior of tannin-modified poly(glycidylmethacrylate)-grafted zirconium oxide-densified cellulose for the selective separation of bovine serum albumin, Colloids Surf. B Biointerfaces 93 (2012) 49–58, https://doi.org/10.1016/j.colsurfb.2011.12.010.
[32] T.S. Anirudhan, J.R. Deepa, Nano-zinc oxide incorporated graphene oxide/nanocellulose composite for the adsorption and photo catalytic degradation of ciprofloxacin hydrochloride from aqueous solutions, J. Colloid Interface Sci. 490 (2017) 343–356, https://doi.org/10.1016/j.jcis.2016.11.042.